Comparison of hybrid Hall thruster model to experimental measurements

Cite as: Phys. Plasmas **13**, 083505 (2006); https://doi.org/10.1063/1.2336186
Submitted: 07 April 2006 . Accepted: 20 July 2006 . Published Online: 31 August 2006

Michelle K. Scharfe, Nicolas Gascon, Mark A. Cappelli, and Eduardo Fernandez

Comparison of hybrid Hall thruster model to experimental measurements

Michelle K. Scharfe, Nicolas Gascon, and Mark A. Cappelli
Stanford University, Stanford, California 94305

Eduardo Fernandez
Eckerd College, St. Petersburg, Florida 33711

(Received 7 April 2006; accepted 20 July 2006; published online 31 August 2006)

A two-dimensional hybrid particle-in-cell numerical model has been constructed in the radial-axial plane with the intent of examining the physics governing Hall thruster operation. The electrons are treated as a magnetized quasi-one-dimensional fluid and the ions are treated as collisionless, unmagnetized discrete particles. The anomalously high electron conductivity experimentally observed in Hall thrusters is accounted for using experimental measurements of electron mobility in the Stanford Hall Thruster. While an experimental mobility results in improved simulation of electron temperature and electric potential relative to a Bohm-type model, results suggest that energy losses due to electron wall interactions may also be an important factor in accurately simulating plasma properties. Using a simplified electron wall damping model modified to produce general agreement with experimental measurements, an evaluation is made of differing treatments of electron mobility, background gas, neutral wall interactions, and charge exchange collisions. Although background gas results in two populations of neutrals, the increased neutral density has little effect on other plasma properties. Diffuse neutral wall interactions are in better agreement with experimental measurements than specular scattering. Also, charge exchange collisions result in an increase in average neutral velocity of 11% and a decrease in average ion velocity of 4% near the exit plane. The momentum exchange that occurs during charge exchange collisions is found to be negligible. © *2006 American Institute of Physics*. [DOI: 10.1063/1.2336186]

I. INTRODUCTION

Closed electron drift Hall thrusters[1] are a plasma propulsion technology receiving considerable attention for their high efficiency. In a typical Hall thruster, electrons travel from an external cathode to an anode at the base of an annular channel. Along their path, the electrons encounter a region of high resistivity due to an imposed radial magnetic field, and become trapped in an $\mathbf{E}\times\mathbf{B}$ Hall current. When neutral particles injected from the anode encounter this region of high electron density, electron impact ionization occurs. The newly born unmagnetized ions then accelerate out of the thruster due to the electrostatic potential maintained between the anode and cathode. While this process results in a high specific impulse device suitable for various low thrust applications, the physics behind these devices is not well understood.

The present study is concerned with the modeling of the interior channel of the Hall thruster and the near-field plume region. A primary challenge in the modeling of channel flow is the treatment of the poorly understood electron conductivity. Since the mobility of electrons affects both the rate of ionization and the accelerating potential, accurately modeling the transport mechanism is critical to developing a practical simulation. However, the experimentally measured mobility of a Hall thruster substantially exceeds the classical value based on electron-neutral collisions.[2] Two possible mechanisms for this anomalous transport are electron wall interactions and azimuthal fluctuations in electron density. Since a radial-axial (r-z) code cannot capture the azimuthal electron dynamics, *ad hoc* transport models are frequently imposed based on Bohm-type diffusion,[3] which scales as the inverse of the magnetic field. In the present study, a comparison is made between a constant Bohm-type transport coefficient and an experimentally motivated axially dependent coefficient.

In addition to electron cross field mobility, results suggest that another factor greatly affecting the simulation of plasma properties is the energy loss due to electron wall interactions. At discharge voltages of 160 and 200 V, a wall damping model assuming isotropic, Maxwellian electrons results in an underprediction of discharge current by more than a factor of 100. Therefore, in this paper we describe a simplified wall damping model in which the energy losses to the walls due to electron impact and secondary electron emission is decreased, producing better agreement with experimental measurements. Additionally, in this paper we examine the effect of neutral wall interactions, background gas, and charge exchange collisions on numerical results. Comparisons are made between the simulation and experimental data in order to assess the validity of the model.

II. NUMERICAL MODEL

A. Assumptions

To aid in the understanding of Hall thruster dynamics, a numerical model has been constructed in the radial-axial plane[4] similar to the model described by Fife.[5] The hybrid model employs a quasi-one-dimensional fluid treatment of electrons and a 2D particle-in-cell (PIC) treatment of the heavy species, Xe and Xe^+. Since the Debye length of a

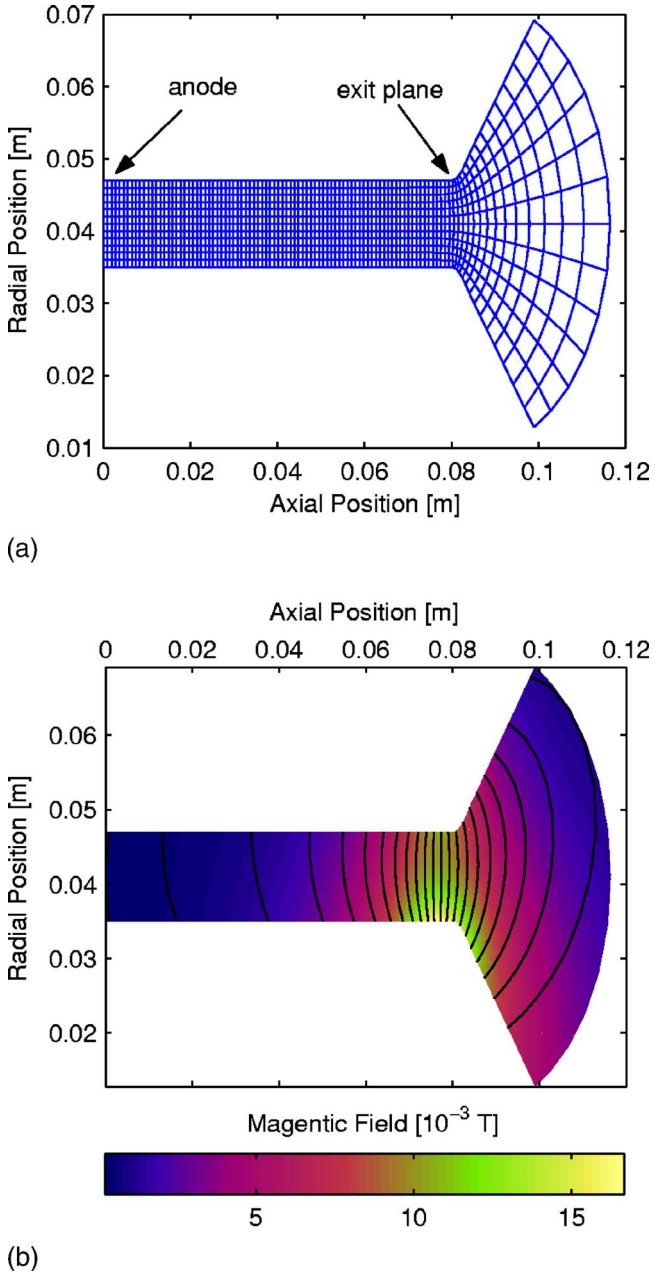

FIG. 1. (Color online) (a) A computational grid of the Stanford Hall Thruster radial-axial simulation. (b) Magnetic field strength (T) and contour lines of the Stanford Hall Thruster.

typical Hall thruster plasma is smaller than the length scales of interest,[6] the two solutions are coupled by assuming space charge neutrality.

The computational geometry used in the simulation corresponds to the laboratory discharge referred to here as the Stanford Hall Thruster, given that extensive experimental data exists for comparison purposes.[7,8] The annular channel is approximately 8 cm in length and 1.2 cm in width. The computational grid, which includes a two-dimensional (2-D) slice of the channel and near field region, is shown in Fig. 1(a). The insulating channel walls are made of alumina. A mass flow rate of 2 mg/s is implemented in the model to match experimental conditions.

Measurements of the magnetic strength in the radial and axial directions along the channel centerline are used to impose a constant external magnetic field, as shown in Fig. 1(b). It is assumed for the results presented that the discharge does not significantly affect the shape or strength of the field. Due to high electron conductivity parallel to the field lines, the electron temperature is assumed to be uniform along magnetic contours.

B. Neutrals

Neutral xenon particles are injected from a region near the center of the anode according to a prescribed mass flow rate of 2 mg/s. The introduced particle velocity distribution is assumed to be that of a Maxwellian one-way flux[9] corresponding to the anode temperature of 1000 K.

Since neutral particles are not affected by electric and magnetic fields, the magnitude and direction of velocity remain the same at each time step, while the azimuthal and radial components of velocity are modified to account for the cylindrical geometry. Particles that exit the computational domain along the channel walls are reflected back into the domain. It is assumed that particles that impact the channel walls thermalize at the wall temperature and are diffusely scattered back into the channel. The wall temperature is assumed to be 1000 K. Similar to anode injection, the velocity distribution of wall scattered neutrals is assumed to be half-Maxwellian. Particles that exit the computational domain in the plume region are no longer tracked by the simulation.

C. Ions

Singly charged xenon ions are generated through electron impact ionization of neutral atoms. The ionization rate is calculated as a function of electron temperature by assuming a Maxwellian distribution of electrons and using experimental cross section data.[10] In addition to increasing the ion population, the ionization process simultaneously depletes the neutral population at each time step. In the present model, only singly charged ions are considered. However, as many as 12% of the ions observed in an SPT-100 have been found to be doubly charged.

Due to their large inertia and Larmor radius, ions are not significantly affected by the external magnetic field. Therefore, the cylindrical equations of motion used to update ion velocities at each time step only include a force due to the transient, spatially varying electric field. Ions that impact channel walls recombine to form neutrals and are diffusely scattered using a half-Maxwellian velocity distribution at 1000 K. Similar to the neutral treatment, ions leave the simulation after crossing the computational boundaries in the plume.

D. Electrons

As outlined by Fife,[5] the electron fluid is governed by the first three moments of the Boltzmann equation in addition to a current conservation equation, assuming quasineutrality.

Neglecting inertial terms and collisional effects, the momentum equation parallel to the magnetic field describes a

balance between electric and pressure forces. Integrating along an isothermal magnetic contour yields an expression for the electric potential, ϕ:

$$\phi = \frac{kT_e}{e} \ln n_e + \phi^*, \tag{1}$$

where ϕ^* is the thermalized electric potential,[11] k is the Boltzmann constant, e is the charge of an electron, T_e is the electron temperature, and n_e is the plasma density. The electric field, $\mathbf{E}$, is then given everywhere in the domain by

$$\mathbf{E} = -\nabla\phi. \tag{2}$$

Perpendicular to the magnetic contours, the electron momentum equation balances electric, pressure, and collisional drag forces. Once again, inertial terms are ignored. An $\mathbf{E}\times\mathbf{B}$ axial force produced by azimuthal electric potential fluctuations interacting with the radial magnetic field is not directly captured in the electron fluid simulation. However, this additional contribution to the axial force is included through an effective experimental mobility and diffusivity in the generalized Ohm's law:[2]

$$u_{e\hat{n}} = -\mu\left(E_{\hat{n}} + \frac{kT_e}{en_e}\frac{\partial n_e}{\partial \hat{n}} + \frac{k}{e}\frac{\partial T_e}{\partial \hat{n}}\right), \tag{3}$$

where $\hat{n}$ indicates the direction normal to the magnetic field, $u_{e\hat{n}}$ is the electron velocity in the normal direction, and μ is the effective mobility.

A transient, spatially varying electron temperature is determined using the second moment of the Boltzmann equation characterizing energy transport:

$$\frac{\partial}{\partial t}\left(\frac{3}{2}n_e kT_e\right) + \frac{\partial}{\partial \hat{n}}\left(\frac{5}{2}n_e u_{e\hat{n}} kT_e - K\frac{\partial T_e}{\partial \hat{n}}\right) = -\dot{n}_e \varphi(T_e) E_i - \Gamma_w + j_{e\hat{n}} E_{\hat{n}}. \tag{4}$$

In the above expression, K is the thermal diffusivity, which incorporates the anomalous electron transport coefficient through the measured mobility. The terms on the right hand side of Eq. (4) represent the ionization and wall damping sink terms and the joule heating source term. The ion production cost, $\varphi(T_e)$, is fit using an exponential expression given by Dugan *et al.*,[12] and is evolved in the original nonlinear form. The term Γ_w represents the energy loss due to the electron flux to the wall.

Presently, the wall damping model is based on an energy dependent secondary electron emission yield assuming alumina walls. As described by Barral *et al.*,[13] the energy dependence is assumed to be linear with an asymptotic total electron emission yield of 0.57 for alumina and a crossover energy of 18 eV. If the electron distribution is assumed to be Maxwellian and isotropic in the bulk, then the average energy of an electron capable of overcoming the sheath barrier is given by $2kT_e + e\phi_w$, where ϕ_w is the difference between the bulk potential and the wall potential. Accounting for the deceleration that occurs when an electron impacts the channel wall, the total electron emission yield is therefore given by

$$\delta(T_e[\mathrm{eV}]) = 0.57 + \frac{2T_e}{18\ \mathrm{eV}}. \tag{5}$$

Unlike the analysis done by Barral *et al.*,[13] a separate electron temperature parallel to the magnetic contours is not simulated. Therefore the bulk temperature is assumed to be isotropic in calculating the secondary electron emission. It is also assumed that inside the sheath and presheath, collisions are not sufficient to maintain a Maxwellian distribution. Therefore, in these regions the electron distribution is assumed to be a shifted and truncated Maxwellian corresponding to the original temperature.

The wall potential is calculated by equating the net electron and ion fluxes to the wall, where the factor of $\exp(-1/2)$ is a result of applying the Bohm criteria for the ion velocity.[14,15] Since the presheath is not directly simulated, the analysis simply assumes that the ions accelerate from their simulated velocity along the edges of the computational domain to the Bohm velocity before striking the walls:

$$\phi_w = \frac{kT_e}{e}\ln\left(\frac{1-\delta}{\exp(-1/2)}\sqrt{\frac{m_i}{2\pi m_e}}\right). \tag{6}$$

As described by Barral *et al.*,[13] space charge saturation occurs when the electron emission yield reaches 0.98. In the space charge saturation regime, the potential is taken to be

$$\phi_w = 1.02\frac{kT_e}{e}. \tag{7}$$

Once the wall potential has been determined, the electron flux to the wall is calculated, again assuming a Maxwellian, isotropic distribution in the bulk. Following the model presented by Barral *et al.*[13] for the alumina channel, it is assumed that 57% of electrons striking the wall are backscattered electrons, which are assumed to retain 60% of their primary energy. The remaining fraction of the secondary electron emission is assumed to be true secondary electrons that lose all of their incoming kinetic energy to the wall. However, both populations are assumed to gain energy equal to the sheath potential when they reenter the bulk. Therefore the net energy density loss is given by

$$\Gamma_w = \frac{2}{L}\exp(-1/2) n_e \sqrt{\frac{kT_e}{m_i}} \times [2kT_e + \phi_w - (\delta e\ \phi_w + 0.57 \times 0.6 \times 2kT_e)], \tag{8}$$

where L is the length of the magnetic contour between the walls, n_e is the bulk electron density, and $\sqrt{kT_e/m_i}$ is the Bohm velocity. The factor of 2 accounts for the losses to both walls.

Assuming space charge neutrality, the electron density is everywhere equal to the ion density, n_i. In order to enforce electron continuity, a total discharge current conservation constraint is imposed:

$$I_a = e\int_A n_e(u_{i\hat{n}} - u_{e\hat{n}})dS, \tag{9}$$

where A is the channel cross section.

A combination of Eqs. (1)–(3) and substitution into the current conservation equation yields an expression for the thermalized potential, ϕ^*, in terms of electron temperature. Therefore, by obtaining the electron temperature through direct solution of the energy equation, the spatially varying electric field, electron velocity, and ionization rate can be calculated at each time step.

E. Solver details

The computational domain of the simulation extends from the anode through the channel and into the near-field plume region. A nonuniform grid is used to span the computational domain with 101 grid points in the axial direction and 13 in the radial direction, as shown in Fig. 1(a).

The numerical model implements a fourth order Runge-Kutta scheme to solve the electron energy equation in order to update the electron temperature perpendicular to the magnetic field at each time step. The spatial derivatives are calculated using second-order central differencing. The boundary conditions used in this implementation are Dirichlet for the electric potential at both the anode and cathode. The temperature boundary conditions are Dirichlet at the cathode assuming constant electron energy injection, and Neumann at the anode assuming infinite diffusion.

For computational manageability, superparticles are used to represent large groups of neutrals and ions rather than simulating individual particles. Since neutral and ion densities differ by orders of magnitude over the length of the domain, the size of the superparticles vary with both space and species. The simulation is initialized with approximately 400 000 superparticles of each heavy particle species. The equations of motion of the heavy particles are solved numerically using a second-order Runge-Kutta scheme.

Due to the fast electron time scale relative to the ions and neutrals, the step size used for time advancement differs for each species. The ion and neutral time step is typically 25 ns, while the electron time step is 0.1 ns. Therefore, ions and neutrals are advanced in time after several electron iterations. On a 3.8 GHz Pentium 4 processor, the simulation completes 625 μs in one day. Over this duration, the simulation undergoes approximately five to ten oscillations in discharge current, reproducing the experimentally observed "breathing mode"[16] cycle. The 10 kHz fluctuation seen in the current is also observed in the plasma density, and is related to an instability in neutral density caused by ionization. This instability leads to a perturbation in the discharge current and plasma density of approximately 10%–12% of the time averaged value. The time averaged plasma density is shown in Fig. 2. Note that this figure also illustrates the 2-D, radial-axial nature of the simulated results.

III. RESULTS AND DISCUSSION

The effect of cross-field mobility, background gas, neutral wall scattering, charge exchange collisions, and discharge voltage on the simulated results will be examined. The reference case will be taken as a 200 V simulation with an experimentally based mobility, diffuse neutral wall interactions, and no background gas or collisions.

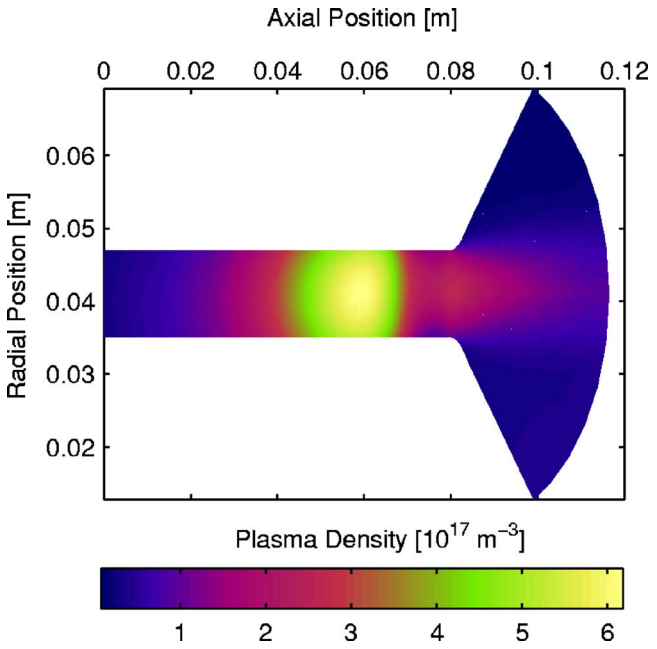

FIG. 2. (Color online) Time averaged plasma density with discharge voltage of 200 V.

A. Electron wall damping

Before the effects of parameters such as charge exchange collisions and background pressure can be assessed, it is necessary that the simulation reasonably predicts experimental measurements within experimental uncertainty. When the model is implemented as described in Sec. II, the discharge current is simulated to be less than 0.01 A, which is more than a factor of 100 lower than the measured value of 2.7 A. Clearly, a discrepancy exists between the simulated physics and the actual behavior of the thruster. Recall that in the present simulation, the presheath is modeled rather than directly simulated. As shown by Ahedo *et al.*,[17] accurately capturing this presheath region is necessary in order to accurately describe the energy transfer at the wall, which may affect properties such as discharge current. Therefore, future work will involve improving the accuracy of the electron wall interactions through direct simulation of the presheath. By refining the grid near the wall and implementing appropriate weighting methods as described by Escobar *et al.*[18] the energy loss mechanism due to electron wall interactions will be more consistent with simulated results near the edges of the computational domain. However, for the purposes of this work, the simple model that assumes that the edges of the computational domain are the beginning of the presheath will be implemented, and other *ad hoc* factors will be examined and tested to improve the agreement with experiment.

One possible factor contributing to the discrepancy between simulated and measured discharge current is that experimental error in the measurements propagates into the experimental mobility, which is dependent on the plasma density, electric potential, and ion velocity. While the ion velocity is experimentally measured with great accuracy using laser induced fluorescence,[7] the plasma density and electric potential are determined using intrusive electrostatic

probe measurements and are therefore not known with as much certainty. The greatest amount of experimental error is likely in the measured plasma density. If the experimental mobility is recalculated by lowering the plasma density in the ionization zone by no more than a factor of 2, the average anode current is simulated to be 0.5 A. This value is more than a factor of 50 greater than the current found using the original mobility. However, since this current is still more than a factor of 5 lower than the experimentally measured current, there are clearly other issues that are not well understood.

Another possible explanation for the discrepancy between the simulated and measured anode current is a violation of the isotropic, Maxwellian electron assumption.[11,19] Only high energy electrons are able to penetrate the sheath and strike the channel surfaces. As described by Meezan *et al.*,[20] the energy transfer rate between electrons is not large enough to replenish the high velocity tail, resulting in a lower electron flux to the wall than predicted by a Maxwellian distribution. However, even if the flux were to remain the same, the non-Maxwellian, anisotropic nature of the electron distribution may also have a large effect on the energy lost per collision. In order for an electron to strike the wall it must have a velocity perpendicular to the wall that satisfies

$$v_{e\perp} > \sqrt{\frac{2e\phi_w}{m_e}} \tag{10}$$

in order to overcome the potential barrier in the sheath. It is assumed that when this particle impacts the wall, the components of velocity in the direction parallel to the wall are chosen randomly from a Maxwellian distribution such that the average energy in each parallel direction is $\frac{1}{2}kT_e$. When the electron strikes and a true secondary electron is emitted, it is assumed that the electron loses all its energy in all three directions. Therefore, when the secondary electron reenters the bulk, it carries with it exactly $e\phi_w$ of energy perpendicular to the wall and no energy in the other two directions. If this electron did not undergo any collisions between the two walls, it would strike the opposite wall and transfer almost no energy. Therefore, the actual amount of energy transferred during an electron collision with the wall is somewhere between the Maxwellian value of $2kT_e$ and 0. If we assume that the average energy transferred to the wall is $0.8kT_e$ when calculating the secondary electron emission yield and net energy loss, then the simulated anode current is 1.6 A.

Each of these mechanisms alone is not enough to explain the discrepancy between the simulated and experimental anode current. Therefore, the real reason for the difference is likely due to some combination of experimental error, anisotropy, non-Maxwellian electrons, and other factors not considered. If we combine the effect of experimental error on the measured plasma density as described above with the effect of non-Maxwellian, anisotropic electrons, then the average simulated anode current is 2.6 A, which is very close to the measured value of 2.7 A. However, since at present the importance of each of these mechanisms is not quantifiable, for the purposes of this paper we will simply introduce an "effective" temperature of $0.4T_e$ when calculating the electron wall damping such that the energy lost per particle is $0.8kT_e$. Recall that this method only produces a simulated anode current of 1.6 A. Although this method is no more justified than other mechanisms for improving the anode current, by making this change the simulation predicts plasma properties with reasonable accuracy, and is sufficient, if not ideal, for analyzing the effects of changing parameters in the simulation.

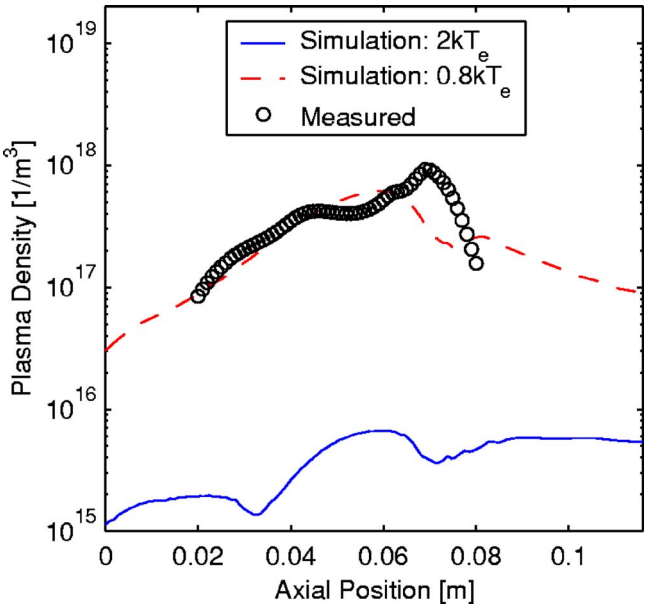

FIG. 3. (Color online) A comparison of experimental plasma density with simulation for electron wall collision energies of $2kT_e$ and $0.8kT_e$.

As shown in Figs. 3 and 4, by assuming that the average energy lost to the wall during electron impact is $0.8kT_e$ instead of $2kT_e$, the simulation is in much better agreement with experiment. For the case of $2kT_e$ energy loss, the simulated plasma density is almost two orders of magnitude lower

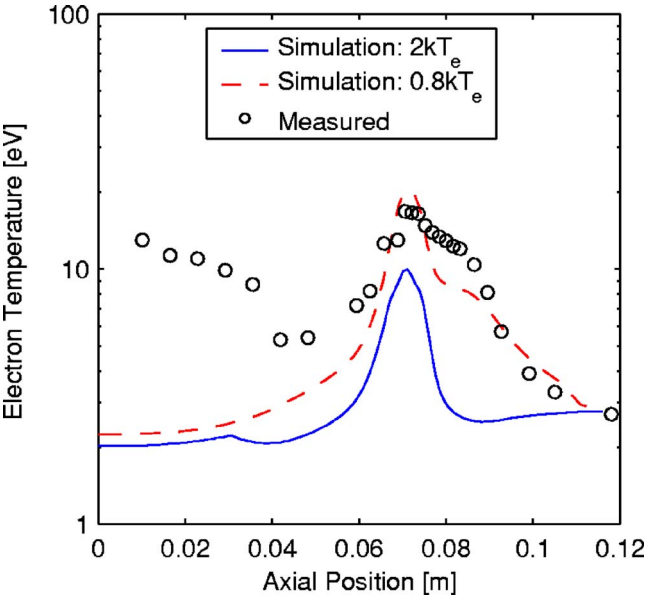

FIG. 4. (Color online) A comparison of experimental electron temperature with simulation for electron wall collision energies of $2kT_e$ and $0.8kT_e$.

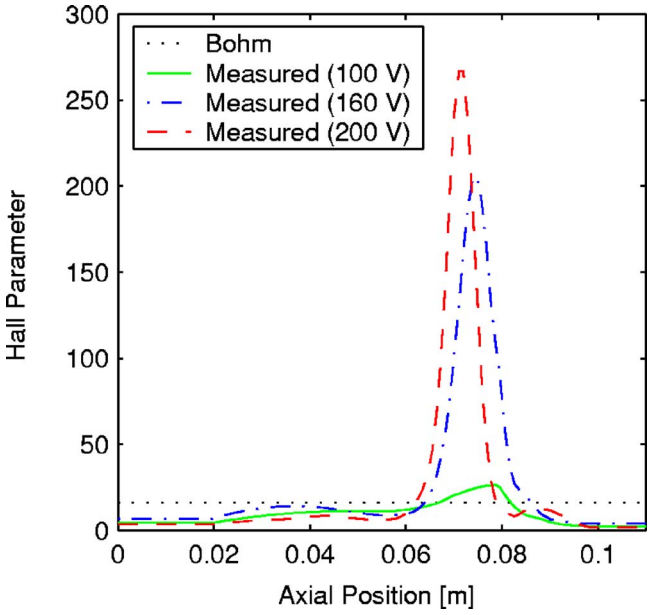

FIG. 5. (Color online) Bohm and experimentally measured Hall parameter $\omega_{ce}\tau$.

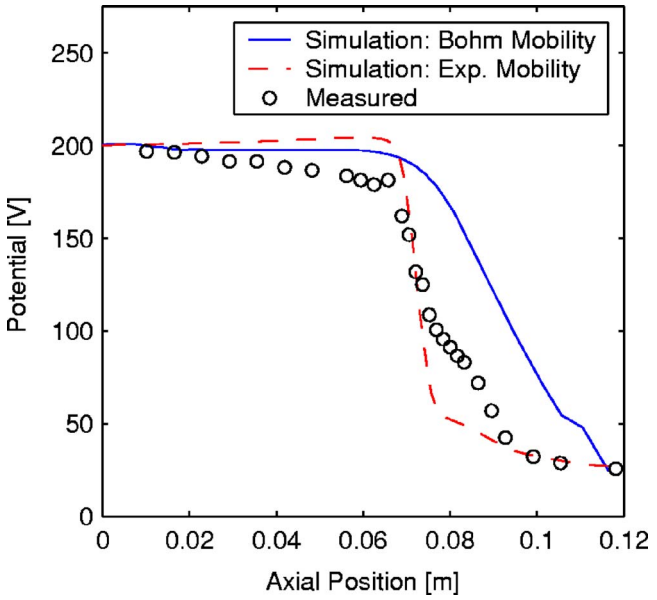

FIG. 6. (Color online) A comparison of experimental potential to the simulated results using Bohm and experimental mobility.

than experimental measurements. Near the channel exit, the simulated electron temperature is also nearly a factor of 10 too low. By lowering the average energy of an incident electron on the wall, all plasma properties can be brought to within reasonable agreement with experiment. Note that the discrepancy near the anode in the electron temperature is most likely due to an inability of the code to capture the glow discharge in this region at 200 V.

B. Cross field mobility

Accurately representing electron diffusion in a numerical model is necessary in order to correctly describe the ionization and acceleration process. However, the experimentally observed axial electron current in a Hall thruster is greater than predicted by classical diffusion based on collisions with neutrals. Since a two-dimensional model is unable to accurately predict the "anomalous" mobility caused by three-dimensional effects such as azimuthal fluctuations, implementation of an *ad hoc* Hall parameter is required.

Classically, cross-field electron mobility is given by

$$\mu_{ez} = \frac{1}{\omega_{ce}\tau B_r}, \tag{11}$$

where B_r is the radial component of the magnetic field, ω_{ce} is the electron cyclotron frequency, and τ is the mean time between collisions.[15] Therefore, electron mobility is inversely proportional to the Hall parameter, $\omega_{ce}\tau$.

According to the Bohm *et al.*[3] model of electron diffusion, the effective Hall parameter is given by $\omega_{ce}\tau = 16$. A comparison of Bohm mobility with an axially varying experimental Hall parameter measured by Meezan *et al.*[20] is given in Fig. 5. As illustrated, the Bohm model fails to capture the significant reduction of cross-field mobility in the ionization region of the channel where the measured mobility is slightly closer to the classical value. Using simulated collision rates, at a discharge voltage of 200 V the classical Hall parameter in the ionization zone is about 7000 versus the experimental value of 270 and the Bohm value of 16.

As shown in Fig. 6, the experimental Hall parameter produces a steep potential drop near the exit plane of the thruster due to the decreased mobility. Using a constant Bohm Hall parameter produces a more gradual accelerating potential that occurs almost entirely outside the channel, also shown in Fig. 6. Although both Bohm and experimental conductivity models fail to reproduce the measured potential, the experimental Hall parameter more accurately confines the acceleration zone, resulting in improved simulation of the electron temperature.

Bohm diffusion produces an electron temperature profile that peaks downstream of the experimentally observed location, as shown in Fig. 7. However, the implementation of an experimental mobility produces electron temperatures that peak at the expected location near the exit plane. The failure of the Bohm model is due in large part to the simulated electric field. For the experimental mobility case, the electric field is largest at the location of the maximum temperature, as shown by the steep gradient of potential in Fig. 6. Since temperature is coupled to the electric field through the Joule heating source term in the energy equation, the location of the maximum electron temperature is correctly predicted for the case of the experimental mobility. However, for the Bohm case, the electric field is less intense in the ionization zone than experimentally measured and more intense in the near field. As a result, the electron temperature is underpredicted in the channel and overpredicted in the plume. A primary factor contributing to the differing potential and temperature curves for the two conductivity models is the inclusion of the experimental mobility in the energy equation through thermal diffusivity, in addition to the generalized Ohm's law. An additional factor contributing to the shift in electron temperature is the increase in discharge current ac-

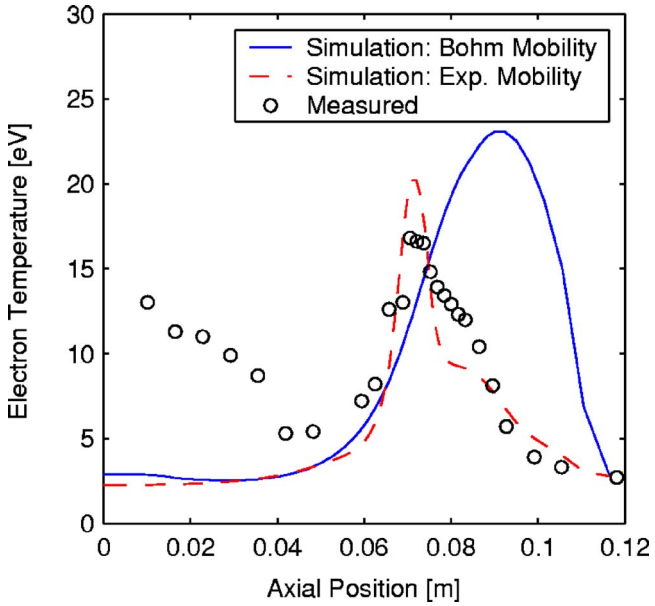

FIG. 7. (Color online) A comparison of experimental electron temperature to the simulated results using Bohm and experimental mobility.

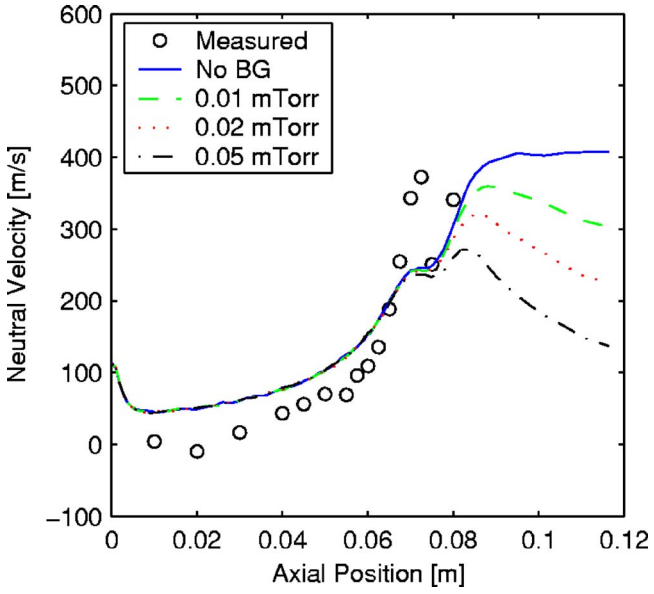

FIG. 8. (Color online) A comparison of experimental axial neutral velocity to simulated results with and without background gas.

companying Bohm diffusion due to the lowered resistance. The enhanced current depletes the neutral population inside the channel through increased ionization, resulting in less ionization-induced losses in the plume.

C. Background

In simulations of ground-based chamber tests, the inclusion of background gas is critical in order to accurately represent the neutral number density. The amount of neutral gas in the simulation is used to calculate the ionization rate, which is directly coupled to the plasma density and electric potential. In order to deduce the magnitude of background effects, background gas has been added to the reference case for comparison. The addition of background gas is accomplished by uniformly injecting neutral xenon particles into the simulation from the edges of the computational domain bordering the near-field region. A net one-way flux of $n\bar{c}/4$ is assumed with a half-Maxwellian velocity distribution normal to the injection surface.

The effect of background gas on the axial neutral velocity is shown in Fig. 8 for background gas at a temperature of 300 K, including the effects of charge exchange. As expected, increasing the amount of back pressure decreases the average neutral velocity since the background population of neutrals travels primarily toward the anode. Also, the ingestion of neutral particles into the channel from the plume results in a 20% increase in neutral density at the exit plane. This increase in neutral density along with a slight increase in the electron temperature results in enhancement of the ionization rate causing a 2% increase in the peak plasma density.

Figures 9 and 10 show the effect of 7×10^{-3} Pa or 0.05 mTorr of background gas on the ion and neutral axial velocity distributions along the centerline of the channel, 4 mm outside the thruster. Both distributions have been normalized such that the integral over velocity equals one. For this run, charge exchange was not included. As expected, background gas increases the population of slow moving ions, as shown in Fig. 9, since background neutrals are typically ionized at a lower potential than neutrals injected from the anode. The average axial ion velocity at this location is lowered by 1.8% due to the introduction of background gas. Also, background gas results in two separate populations of neutrals: those injected from the anode, which have a net motion out of the thruster, and those introduced as back-

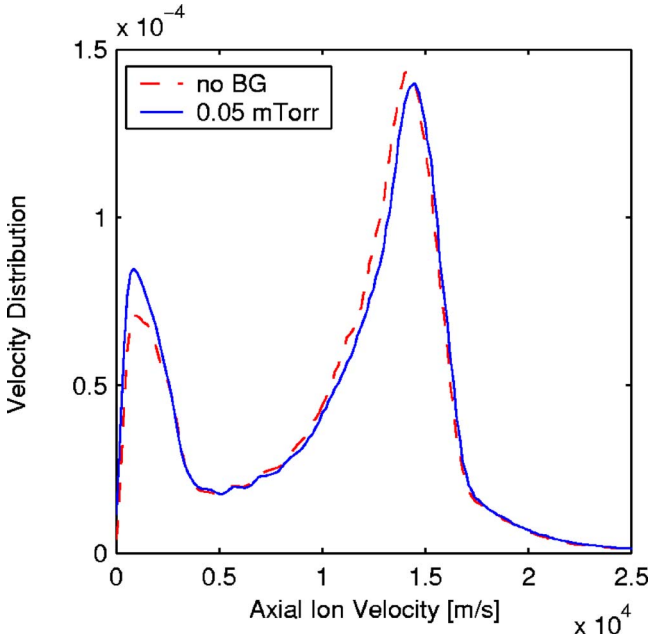

FIG. 9. (Color online) A comparison of axial ion velocity distribution with and without background gas 4 mm beyond the exit plane of the Hall thruster.

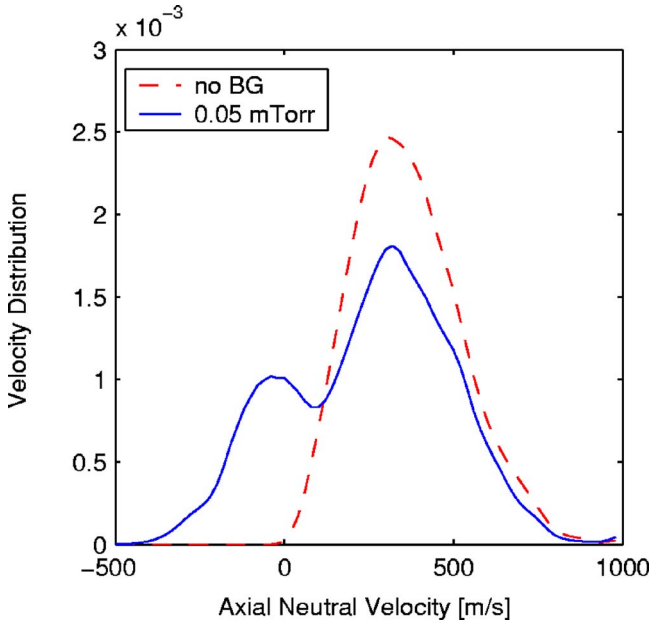

FIG. 10. (Color online) A comparison of axial neutral velocity distribution with and without background gas 4 mm beyond the exit plane of the Hall thruster.

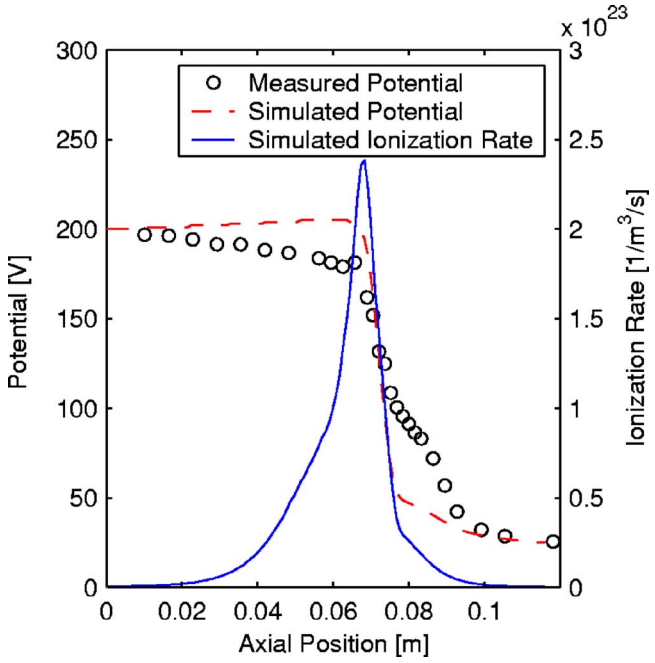

FIG. 11. (Color online) A comparison of experimental and simulated electric potential with a simulated ionization rate along the centerline of the thruster.

ground gas, which have a net motion into the thruster. This doubly peaked distribution shown in Fig. 10 lowers the average neutral velocity by 31.8%.

Another key feature to recognize in Fig. 9 is that even without background gas there is a significant population of low energy ions. Experimentally, as reported by Cedolin,[21] a tail of slow moving ions is observed. However, Cedolin does not measure a second local maximum at low velocities. Hagelaar *et al.*[22] have attributed a similar low energy population to transit time oscillations. In this case, however, the reason for the discrepancy with experiment is believed to be a simulated potential drop that is too steep, as shown in Fig. 11. A small amount of ionization is still occurring near the thruster exit, located 8 cm downstream of the anode. In the simulation, these newly born ions are near the bottom of the potential well and the accelerating electric field is small. However, experimentally, nearly half the potential drop occurs outside the thruster. By the time the electric field is small, it is likely that the amount of ionization is negligible.

D. Neutral wall interactions

The way in which neutral particles reflect off the channel walls directly affects the neutral velocity profile and the neutral number density in the entire computational domain.[23] Since neutral density is coupled to plasma density through ionization, neutral wall interactions are relevant to the overall accuracy of the simulation. The two primary models for neutral wall interactions are specular and diffuse scattering. Each method is implemented separately in the simulation and the results are compared with experimental measurements to determine which model better reflects reality. Specular scattering is accomplished by reversing the radial component of velocity when a particle reaches the channel boundaries. In diffuse scattering, the particle thermalizes at the wall temperature and is reemitted at a random angle and with a speed chosen using a Maxwellian one-way velocity distribution function.

Specular scattering produces a neutral number density that is far more uniform inside the channel than in the diffuse scattering case. For the outer half of the channel, the diffuse scattering simulation matches experimental observations well, whereas the specular scattering overestimates the neutral number density by as much as 40%. As a result of this increased neutral density in the ionization zone, the peak plasma density is approximately doubled for the specular case.

Experimentally, the axial neutral velocity is observed to be small near the anode. As shown in Fig. 12, diffuse scattering, which tends to randomize the neutral velocity, produces better agreement with experiment than specular scattering. Both wall interaction models produce the observed increase in axial velocity near the exit due to the preferential removal of slow ions from the distribution caused by ionization. The overall better agreement of diffuse scattering relative to specular scattering is consistent with work done by Vial *et al.*[23]

E. Charge exchange collisions

To better understand the plasma dynamics that occur inside a Hall thruster, the effect of heavy particle interactions has been studied through the inclusion of charge exchange collisions. In reality, heavy particle collisions involve the transfer of momentum, and in some cases, an exchange of charge. Pure momentum transfer collisions are neglected in the simulation, since it is assumed that elastic collisions result in only a small change in the velocity distribution function of each species. However, since charge transfer colli-

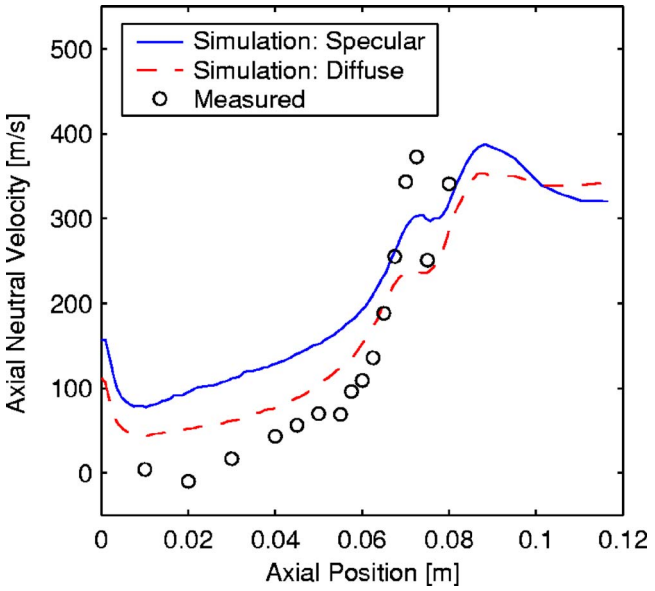

FIG. 12. (Color online) A comparison of experimental axial neutral velocity to simulated results using specular and diffuse wall interactions.

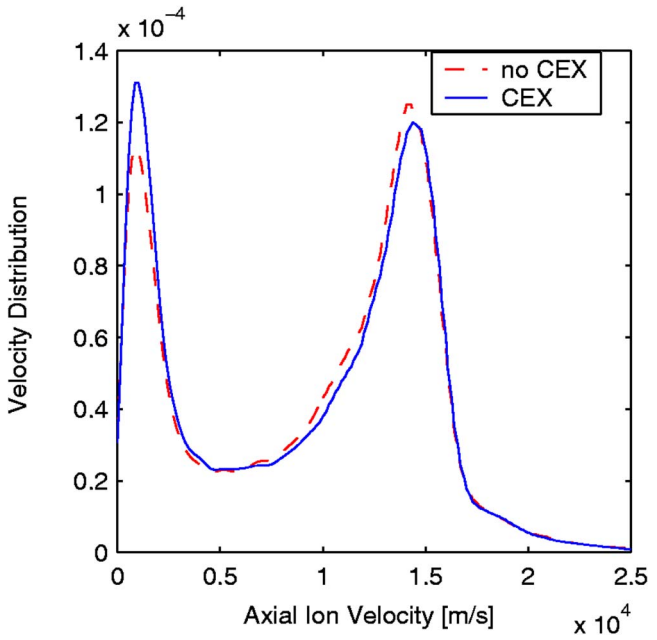

FIG. 13. (Color online) Effect of charge exchange on axial ion velocity distribution at the exit plane.

sions typically produce high velocity neutrals and slow moving ions, this type of collision is studied in depth.

In order to implement charge exchange collisions in the simulation, first collision partners are chosen using the pair selection scheme described by Bird.[24] Only neutrals and ions in the same computational cell are eligible to collide. From within a given cell, X ion-neutral pairs are chosen according to the formula

$$X = n_i n_n (\sigma g)_{\max} V \Delta t, \tag{12}$$

where n_i is the ion density, n_n is the neutral density, $(\sigma g)_{\max}$ is the maximum value of the total cross section multiplied by the relative velocity for all possible pairs, V is the volume of the cell, and Δt is the time step.

Experimental measurements by Miller *et al.*[25] are used to determine the total cross section as a function of energy:

$$\sigma_{\mathrm{Xe-Xe^+}} = \left[87.3 - 13.6 \log_{10}\left(\frac{m_{\mathrm{Xe}} g^2}{2e}\right)\right] \times 10^{-20}\ \text{Å}^2. \tag{13}$$

Once X partners are chosen, they are collided with probability, P, given by

$$P = \frac{\sigma g}{(\sigma g)_{\max}}. \tag{14}$$

Differing superparticle weights are accounted for in selecting collision pairs. On average, a neutral superparticle is two orders of magnitude larger than an ion superparticle. Therefore, if a charge exchange collision is determined to take place, the larger particle (typically the neutral) is divided into a small particle the size of the collision partner and a large particle equal to the remainder. The collision occurs between the two equally sized particles, while the remainder particle retains its precollision velocity. Since the most probable scattering event involves very little momentum transfer, in this discussion momentum transfer is neglected and the precollision velocities of the ion and neutral are exchanged. Previous work using approximate differential cross sections found that the influence of momentum exchange during charge transfer collisions was negligible.[26]

For the specific thruster modeled, it was found that charge exchange collisions predominantly occurred halfway along the length of the channel with a higher frequency of collisions along the inner wall. This location is both upstream of the ionization zone and in the region of a strong electric field.

As shown by Fig. 13, which includes background gas, adding charge exchange collisions to the simulation reduces the number of high velocity ions and increases the number of low velocity ions. Since the probability of a charge exchange collision between two particles decreases with increasing relative velocity, the change in the distribution is statistically insignificant for ion velocities greater than about 18 000 m/s. The average velocity of the ion population at the exit plane decreases from 9649 m/s without charge exchange to 9352 m/s with charge exchange. Therefore, including charge exchange produces a change of nearly 4% at the exit plane. Experimentally, the average ion velocity at the exit plane is measured to be 9165 m/s. The simulated value is higher than the experimental value both with and without charge exchange due to the lower simulated voltage at the exit plane.

Since charge exchange decreases the average ion velocity, as expected charge exchange also increases the average neutral velocity, as shown in Fig. 14. The average simulated neutral velocity at the exit plane increases from 244 m/s without charge exchange to 273 m/s with charge exchange. Therefore, charge exchange produces an 11% increase in the neutral velocity at the exit plane. Although the experimental axial neutral velocity at the exit plane is 341 m/s, it is not

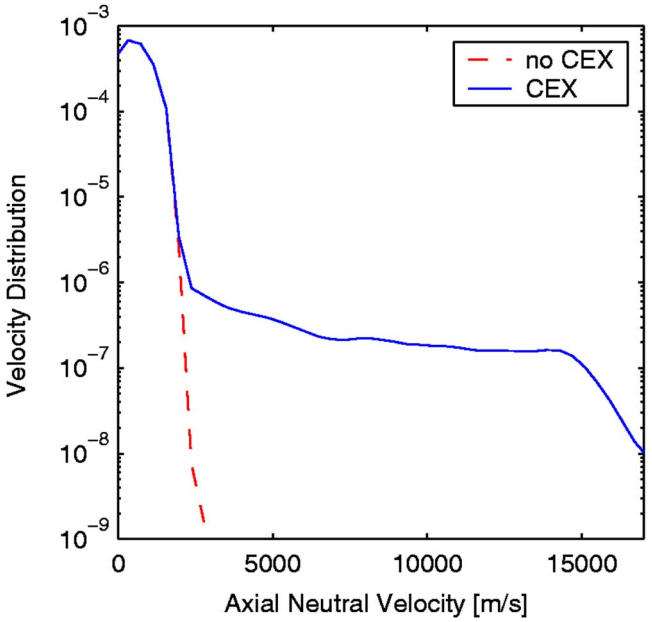

FIG. 14. (Color online) Effect of charge exchange on axial neutral velocity distribution at the exit plane.

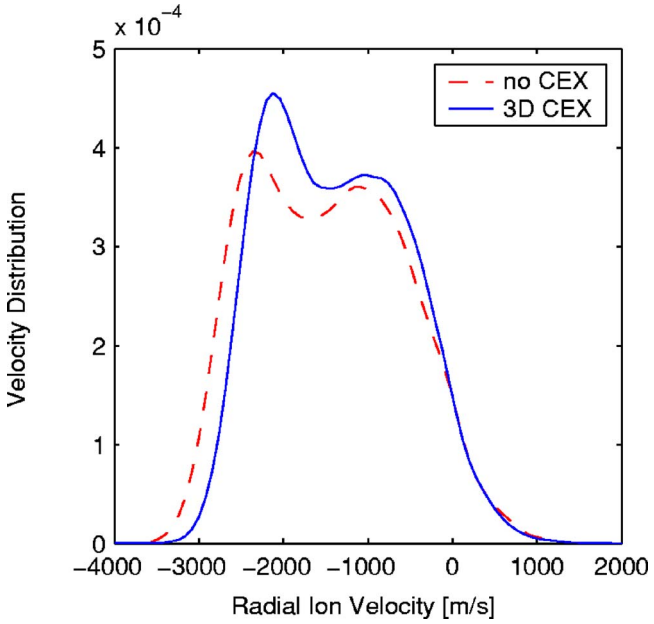

FIG. 15. (Color online) Effect of charge exchange on radial ion velocity distribution at the exit plane at a radial position aligned with the inner channel.

valid to compare the experimental value with the charge exchange case. As shown in Fig. 14, rather than shifting the Gaussian peak, charge exchange instead adds a high velocity tail to the velocity distribution. Since the past laser induced fluorescence measurements did not encompass these high velocities, the experimental average would not include such particles. One possible explanation for an experimental value higher than the simulated values is that the simulated background flux may be too high. Although the pressure is measured to be 1.3×10^{-2} Pa or 0.1 mTorr by an ion gauge at the end of the chamber, it is possible that the actual pressure near the thruster is not equal to this value. If less background gas is present, the average neutral velocity exiting the thruster would increase. However, even in the limiting case of no background gas, the velocity at the exit plane is only 306 m/s, as shown in Fig. 8. Another factor contributing to the underestimation of neutral velocity is the narrowness of the temperature profile relative to experimental measurements, as shown in Fig. 7. Since ionization selectively removes slow ions, a wider temperature profile would further increase the neutral velocity.

Using the implemented charge exchange model, the effect of these collisions on plasma properties and velocity distributions can be critically examined both in the interior channel and in the near field region. It is commonly believed that charge exchange may be a significant factor contributing to spacecraft degradation.[27] Neglecting background gas, the probability of an ion having a velocity of 1 km/s increases by 18% due to charge exchange collisions. Note that in reality this probability may be even higher due to the artificially large low-energy population produced by the simulation. Collisions also result in a 4% increase in the percentage of the population moving slower than 5 km/s. An increase in the number of slow-moving ions is a cause for concern, because these particles are more likely to be influenced by stray fields that may be present on an actual spacecraft. If a slow-moving ion is accelerated back toward critical spacecraft components, it could lead to sputtering and deposition.

In the interior channel of the thruster, as expected, the backflow of ions toward the anode is reduced due to the impedance added by collisions. Experimentally, the backflow is measured to be 230 m/s along the centerline for a 200 V discharge voltage. Without collisions, the simulated value is 1200 m/s, while the inclusion of charge exchange reduces the value to 725 m/s. The reason for the large backflow is a simulated electric field upstream of the ionization zone that accelerates the ions back toward the anode. In fact, the inclusion of charge exchange collisions causes this reverse field to increase near the anode by 20%. Collisions also result in a reduction of electron temperature near the anode of 3%. This lowered temperature in the first 2 to 3 cm of the channel, combined with a lowered neutral density in most regions of the channel, results in lower ionization, causing a reduction of the peak plasma density by 2% and a reduction of 55% at the anode. However, although the plasma density is either reduced or remains constant everywhere inside the channel, the neutral density increases by as much as 9% near the inner wall and the peak ionization rate increases by 23%. It is thought that the extra ions lead to an increase in the flux of ions to the wall. Upstream of the ionization zone, the radial velocity into the inner wall increases by as much as 50%. However, along the outer wall the radial velocity decreases by as much as 20%. Conversely, beyond the ionization zone, the average radial velocity toward the inner wall decreases, as shown in Fig. 15. Along the outer wall, the reverse is true and the average radial velocity increases. The asymmetry observed may be a result of the collisional enhancement of asymmetry already present in the thruster. Without collisions, a radial electric field along the centerline

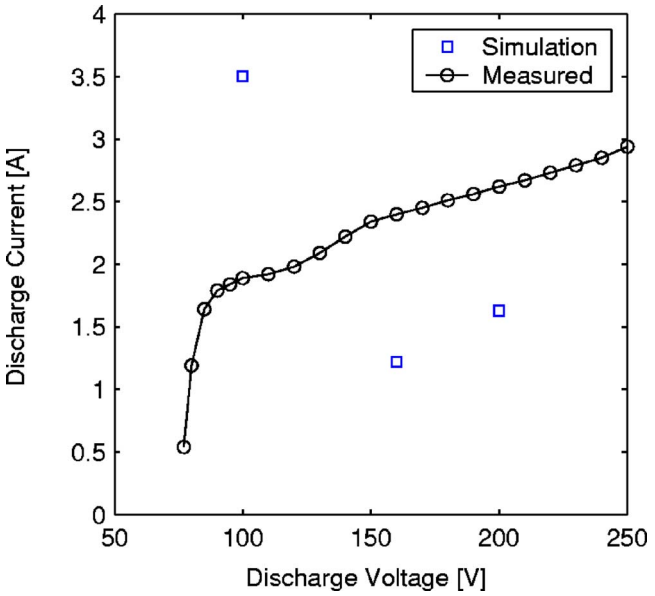

FIG. 16. (Color online) A comparison of simulated discharge current with experimental measurements at 100, 160, and 200 V.

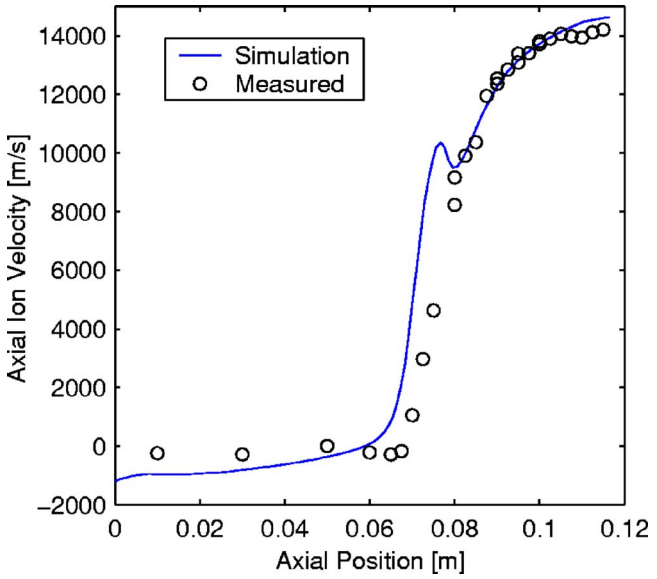

FIG. 17. (Color online) Simulated ion velocity for the reference case versus experimental ion velocity.

of the channel is present that accelerates the ions outward. Since particles with comparable velocities are more likely to collide, this causes charge exchange to occur more frequently along the inner wall. Therefore, the nonuniformity of the collisions leads to a number of slight changes in the plasma that are only indirectly related to the collisions themselves.

F. Discharge voltage

The robustness of the numerical model has been tested through variation of the applied discharge voltage. The simulation was run at 100 V, 160 V, and 200 V corresponding to discharge voltages at which electron mobilities have been experimentally determined.

At 160 and 200 V, the simulated current is nearly 50% lower than experimentally measured, as shown in Fig. 16. As discussed in Sec. III A, if the experimental number density is lowered and the mobility recalculated in addition to lowering the electron wall damping, then the simulated anode current is 2.6 A at 200 V, which is in good agreement with experimental measurements. This suggests that either the experimental mobility is too low, or the damping mechanisms such as electron wall interactions have too large an effect.

While the simulation predicts similar discrepancies from experiment at 160 and 200 V, the simulated results at 100 V overpredict the discharge current by 80%, suggesting that new physics needs to be added for lower voltages. Note that the same wall damping models were used at all three voltages. While lowering the amount of energy transferred during an electron wall interaction may be appropriate at higher voltages, it is possible that at lower voltages the electron energy distributions remain nearly Maxwellian, resulting in the full $2kT_e$ of energy being lost to the walls.

G. Particular features

As shown by the axial ion velocity in Fig. 17, in addition to reproducing the overall acceleration process with reasonable accuracy, the simulation also captures the subtle physical phenomena observed experimentally. The simulation predicts a backward acceleration of ions toward the anode upstream of the ionization zone. This characteristic of the ion velocity has been experimentally observed in the Stanford Hall Thruster using laser induced fluorescence measurements.[7] At 200 V, the reference case simulation produces average velocities on the order of 1000 m/s in the reverse direction near the anode. Experimentally, a net backflow is observed at the same operating conditions, however, the magnitude of the reverse flow is a factor of 5 lower than predicted by the simulation.

Also in Fig. 17, the simulation predicts a dip in the ion velocity near the exit plane. While this dip is not apparent at 200 V, a slight decrease in the acceleration is observed near the same location. As reported by Hargus,[7] a more noticeable kink is apparent in the axial ion velocity of the Stanford Hall Thruster at a higher operating voltage of 250 V. The feature is likely a result of the decreased accelerating potential in this region (Fig. 6) being unable to overcome the axial velocity losses due to wall interactions and ionization. A consequence of the sudden decrease in ion velocity is a slight increase in the simulated plasma density at the same location as shown in Fig. 3.

Another experimentally observed phenomena which the simulation is able to reproduce is a decrease near the exit plane of the axial neutral velocity, as shown in Fig. 18. The shape of the axial velocity curve is influenced by the ionization rate and diffuse wall interactions. While the ionization process selectively removes slow neutrals from the distribution, diffuse wall interactions impede the neutral flow. After the accelerating ionization influence drops off, as shown in Fig. 18, the wall interactions cause the neutral velocity to

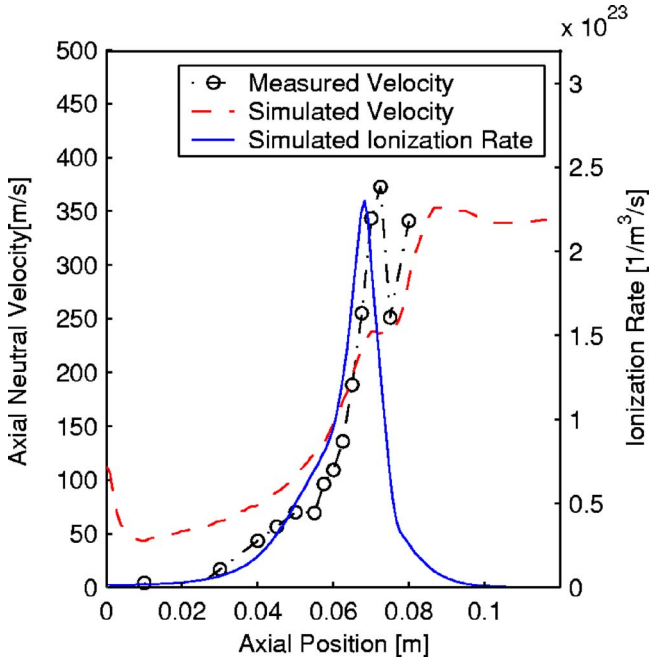

FIG. 18. (Color online) Simulated ionization rate and neutral velocity for the reference case versus experimental neutral velocity.

fall. Near the exit plane, the average velocity increases once again due to a lack of particle flux in the opposing direction.

IV. SUMMARY

It has been shown that using an experimentally measured Hall parameter to describe the anomalous nature of electron cross-field mobility produces discharge properties that are in better agreement with experimental measurements than a Bohm-type model. Also, this work has shown that diffuse neutral wall interactions produce better neutral density and velocity profiles than specular scattering. Background effects have been shown to increase the population of slow moving ions and produce a population of neutrals moving toward the anode. At the exit plane, charge exchange appears to affect the average ion velocity by 4% and the neutral velocity by 11%. Farther downstream, the effect is simulated to be even greater, but the reliability of the simulation near computational boundaries is questionable. However, despite a possible lack of accuracy, an increase in the low-energy population of ions is clearly observed in the near field region, and is possibly significant in understanding spacecraft degradation.

One of the key successes of this numerical model is the ability to reproduce subtle experimentally observed features. Although the phenomena are exaggerated in the simulation, the model predicts a backflow of ions near the anode and a kink in axial ion velocity near the exit plane. In addition, the simulation accurately reproduces the exact location of an experimentally measured dip in axial neutral velocity caused by the counteracting influences of ionization and diffuse wall scattering.

ACKNOWLEDGMENTS

M.A.C. and N.G. would like to thank Caroline Vialard-Goudou for her contribution to improving the electron diffusion description in the code.

This research was supported by the Air Force Office of Scientific Research. Stipend support for M.K.S. was provided through a fellowship from the National Science Foundation. N.G. was partially supported by a fellowship from the European Space Agency. E.F. acknowledges the Center for Turbulence Research for supporting this work and K. Mahesh for valuable assistance in the early stages of code development.

[1] V. Zhurin, H. Kaufman, and R. Robinson, Plasma Sources Sci. Technol. **8**, R1 (1999).
[2] N. Meezan, W. Hargus, and M. Cappelli, Phys. Rev. E **63**, 026410 (2001).
[3] D. Bohm, E. Burhop, and H. Massey, *The Characteristics of Electrical Discharges in Magnetic Fields* (McGraw-Hill, New York, 1949), p. 13.
[4] E. Fernandez, M. Cappelli, and K. Mahesh, *CTR Annual Research Briefs* (Center for Turbulence Research, Stanford, CA, 1998), p. 81.
[5] J. Fife, Ph.D. thesis, Massachusetts Institute of Technology, 1998.
[6] E. Choueiri, Phys. Plasmas **8**, 1411 (2000).
[7] W. Hargus, Ph.D. thesis, Stanford University, 2001.
[8] N. Meezan, Ph.D. thesis, Stanford University, 2002.
[9] C. Birdsall and A. Langdon, *Plasma Physics via Computer Simulation* (IOP Publishing, Briston, England, 1991).
[10] D. Rapp and P. Englander-Golden, J. Chem. Phys. **43**, 1464 (1965).
[11] A. Morozov and V. Savelyev, Rev. Plasma Phys. **21**, 203 (2000).
[12] J. Dugan and R. Sovie, Tech. Rep. D-4150, National Aeronautics and Space Administration, 1967.
[13] S. Barral, K. Makowski, Z. Peradzynski, N. Gascon, and M. Dudeck, Phys. Plasmas **10**, 4137 (2003).
[14] D. Bohm, *The Characteristics of Electrical Discharges in Magnetic Fields* (McGraw Hill, New York, 1949), p. 77.
[15] F. Chen, *Introduction to Plasma Physics and Controlled Fusion* (Plenum, New York, 1984).
[16] J. Boeuf and L. Garrigues, J. Appl. Phys. **84**, 3541 (1998).
[17] E. Ahedo, Phys. Plasmas **9**, 4340 (2002).
[18] D. Escobar, E. Ahedo, and F. Parra, *Proceedings of the 29th International Electric Propulsion Conference* (The Electric Rocket Propulsion Society, Worthington, OH, 2005), IEPC-2005-041.
[19] A. Bugrova, A. Desyatskov, and A. Morozov, Sov. J. Plasma Phys. **18**, 501 (1992).
[20] N. Meezan and M. Cappelli, Phys. Rev. E **66**, 036401 (2002).
[21] R. Cedolin, Ph.D. thesis, Stanford University, 1997.
[22] G. Hagelaar, J. Bareilles, L. Garrigues, and J.-P. Boeuf, J. Appl. Phys. **93**, 67 (2002).
[23] V. Vial, A. Lazurenko, C. Laure, A. Bouchoule, and D. Pagnon, *Proceedings of the 28th International Electric Propulsion Conference* (The Electric Rocket Propulsion Society, Worthington, OH, 2003), IEPC-03-0221.
[24] G. Bird, *Molecular Gas Dynamics and Direct Simulation of Gas Flows* (Oxford University Press, Oxford, 1994).
[25] J. Miller, S. Pullins, D. Levandier, Y. Chiu, and R. Dressler, J. Appl. Phys. **91**, 984 (2002).
[26] M. Allis, N. Gascon, M. Cappelli, and E. Fernandez, *Proceedings of the 29th International Electric Propulsion Conference* (The Electric Rocket Propulsion Society, Worthington, OH, 2005), IEPC-2005-057.
[27] S. Pullins, Y.-H. Chiu, D. Levandier, and R. Dressler, *Proceedings of the 38th Aerospace Sciences Meeting and Exhibit* (American Institute of Aeronautics and Astronautics, Washington, DC, 2000), AIAA-2000-0603.